Selective edge functionalization of graphene layers with oxygenated groups by means of Reimer-Tiemann and domino Reimer-Tiemann/Cannizzaro reactions

Selective edge functionalization of graphene layers with oxygenated groups by means of Reimer-Tiemann and domino Reimer-Tiemann / Cannizzaro reactions

Vincenzina Barbera[1]*, Luigi Brambilla[1], Alessandro Porta[1], Roberta Bongiovanni[2], Alessandra Vitale[2], Giulio Torrisi,[1] Maurizio Galimberti[1]*

[1]Politecnico di Milano, Department of Chemistry, Materials and Chemical Engineering "G. Natta", Via Mancinelli 7, 20131 Milano, Italy

[2] Politecnico di Torino, Department of Applied Science and Technology, Corso Duca degli Abruzzi 24, 10129 Torino, Italy

Abstract

Graphene layers were selectively edge-functionalized with oxygenated functional groups, maintaining their bulk structure essentially unaltered. A reaction was performed between polyhydroxylated graphene layers (G-OH) and $CHCl_3$/KOH/H_2O. When the reaction with KOH/H_2O was performed at 0°C, by adding successive portions of $CHCl_3$, the functionalization occurred with aldehydic functional groups. When G-OH ~~was~~ reacted with $CHCl_3$/KOH at room temperature, benzylic alcohol and carboxy groups w~~h~~ere introduced. XPS, IR, Raman, WAXD analyses indicated that the graphene layers were chemically modified with the abovementioned functional groups, without intercalated and/or absorbed molecules. It can be thus assumed that functionalization of G-OH with aldehydic groups occurred through Reimer-Tiemann reaction and that domino Reimer-Tiemann / Cannizzaro reaction led to aldehyde disproportion. As a further evidence and a first viable usage of the functionalization with aldehydic functional groups, chitosan was crosslinked with the graphene layers, obtaining flexible and electrically conductive carbon papers.

*Corresponding author. E-mail: vincenzina.barbera@polimi.it (Vincenzina Barbera)

*Corresponding author. E-mail: maurizio.galimberti@polimi.it (Maurizio Galimberti)

1. Introduction

Graphene [1-3] has indeed exceptional properties: it features high charge-carrier mobilities [4,5], its in-plane thermal conductivity is among the highest for known materials [6], the theoretical elastic modulus is over 1 TPa and the Young modulus is about 1060 MPa [7]. Thanks in particular to their electrical properties, graphene and graphene related materials find application for energy storage devices [8-10] and in fuel cells [11].

Such outstanding graphene properties are essentially due to its six atoms aromatic ring core. Any synthesis [7-15] and functionalization [7, 16-22] has therefore the objective to obtain and preserve such structure. In particular, the control of size, shape, and edge structure of graphene layers is a challenging task.

Graphene functionalization has great importance. Functional groups affect electronic and solubility properties, self-assembly and phase forming behaviour and can promote further reactions. Over the last years, research has been focused on edge functionalization [3-21], so as to preserve the ideal structure of the graphene core. Edge functionalization has been reported with halogen atoms, [20,21,23-26] converted to nitrile [27] or arylthio [28] groups and used for various metal-catalyzed coupling reactions [29]. Iridium-catalysed direct borylation reaction [30], direct palladium-catalyzed C–H arylation [31] and double C–H activation [32], initializing the construction of novel aromatic structures [33], have also been reported.

Great interest is shown for graphene layers with oxygenated functional groups. The chemistry of carboxylic acids has been much explored in the case of carbon nanotubes (CNT) [34]: amidation and esterification reactions have been applied in order to achieve solubility in different solvents, to perform the so-called grafting from polymerizations, to prepare biocompatible sensors. Moreover, graphene and oxygenated derivatives, such as graphene oxide (GO), are being increasingly applied in the field of catalysis [35]. The chemical or thermal reduction of graphene oxide is considered the best practice for large-scale production of graphene [14].

However, the introduction of carboxylic groups on CNT and, in particular, the preparation of GO require strong acidic, harsh and even dangerous oxidative conditions [36-46]. The structure of GO has been investigated for decades, but it is still substantially unknown [7,13]. It has been reported [47] that carbonyl and carboxylic groups are on the edges and hydroxy and epoxy groups are on basal planes. Hence, the chemistry that leads to GO cannot be used for the selective edge functionalization of graphene layers. Alternatively, Friedel–Crafts acylation reaction with 4-aminobenzoic acid was performed: it is a one-pot reaction, but requires acidic substances, which could hardly be removed from a graphitic substrate. Another approach reported in the literature for the edge carboxylation is ball milling with carbon dioxide [48]: ~~the~~ this method is environmentally

friendly, but does not appear ideal for large-scale development. This work describes a new procedure for the edge functionalization of graphene layers with oxygenated functional groups, in particular aldehydes and carboxylic acids or their ester derivatives. It is worth clarifying that reactions were designed to occur on peripheral positions of graphene layers, independently of their organization as single layers or as stacks of few or many layers. Nanosized high surface area graphite (G) with high shape anisotropy (i.e. with a high ratio between the size of crystallites parallel and perpendicular to the structural layers [49]) was chosen as ~~a~~ starting material and the synthetic strategy shown in Figure 1 was adopted.

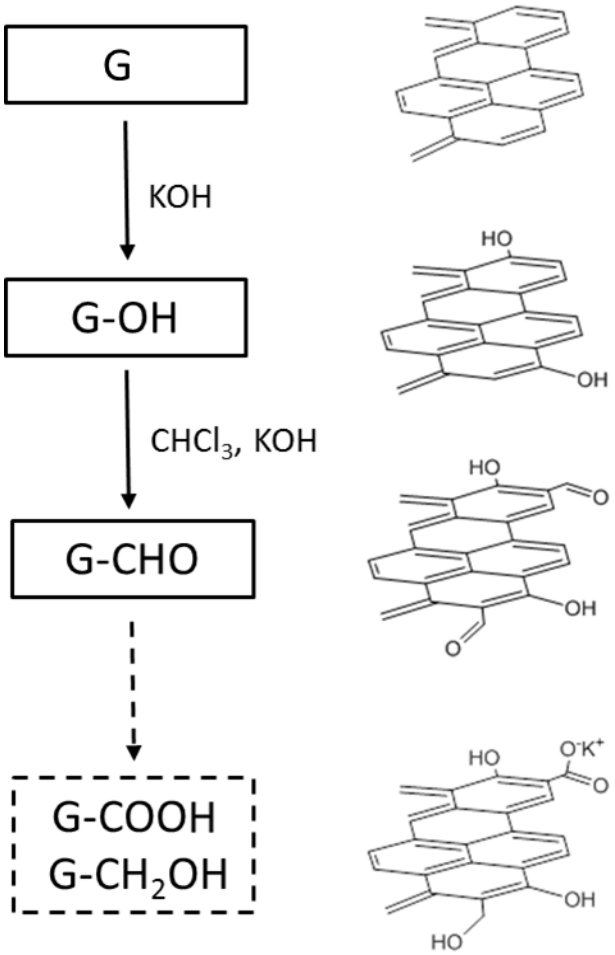

Figure 1. Synthetic strategy for the introduction of oxygenated functional groups on the edges of graphene layers G.

As reported in previous works [50,51], G can be easily functionalised with hydroxyl groups in peripheral position and polyhydroxylated graphene layers are obtained, with substantially unaltered bulk structure. G-OH layers can be considered as a polycyclic aromatic compound, suitable for reactions able to introduce oxygenated functional groups on phenolic substrates. Besides Friedel-

Crafts acylation, Reimer-Tiemann reaction [52,53] has been known for a long time as an efficient tool for the preparation of 2-hydroxyaryl aldehydes [52], and is used on an industrial scale for the preparation of salicylic aldehyde (2-hydroxybenzaldehyde)~~salicylaldehyde~~, an important intermediate in the chemical industry for the production of fragrances, perfumes, dyes and pharmaceuticals. Studies on Reimer-Tiemann reaction [54] have demonstrated that dichlorocarbene, formed by mixing chloroform with KOH, interacts with the potassium salt of the phenolic substrate in the aqueous phase. By using the same reaction mixture, $CHCl_3$ in alkaline medium, in the presence of a phase transfer catalyst, cyclopropanation reaction occurs on alkenylic substrates [55] and at the edges of graphene layers [56]. These reagents are not the preferred ones, as cyclopropanes are traditionally formed by adding the methylene–zinc–iodide complex, generated from diethyl zinc and diiodomethane [57-59], or by transition metal-catalyzed decomposition of diazo compounds [60]. As G-OH forms stable water dispersions [51] it could thus be a suitable substrate and graphene layers bearing 2-hydroxy aldehyde as functional group should be obtained. However, the selectivity of the Riemer-Tiemann reaction on G-OH cannot be taken for granted. Indeed, it is well known that a strong base, such as KOH, can induce disproportionation of aromatic aldehydes lacking a hydrogen atom in the α-position, promoting the Cannizzaro reaction and leading to benzyl alcohol and potassium benzoate. However, to obtain disproportionation of aldehyde with vanillin as substrate, a catalyst had to be used [61,62] and electrocatalytic effects have been reported to enhance the efficiency of the Cannizzaro reaction [63]. It has to be taken into account that carbon nanostructured materials such as carbon fibers and carbon nanotubes have been used as catalysts for phenol oxidation [64]. Hence, the occurring of Cannizzaro reaction, indicated with the dotted line in the block diagram in Figure 1, cannot be ruled out. Moreover, the introduction of aldehydes in other positions of the graphene layers, which are indeed electron rich, could also be hypothesized. Rather than stretching too far inferences not supported by experimental facts, in this work G-OH was subjected to the Riemer-Tiemann reaction, performed under ~~with~~ different experimental conditions: at nominal room temperature, reproducing the experimental conditions usually adopted in the prior art, and at 0°C by adding chloroform in three portions, with the aim of preventing the Cannizzaro disproportionation. Mechanisms for the formation of functionalized graphene layers are proposed.

Moreover, reaction of chitosan (CS) with graphene layers bearing aldehydic groups was performed ~~for preparing~~ to prepare bionanocomposites.

2. Experimetal

2.1 Materials and methods

Reagents and solvents were commercially available and were used without further purification: KOH pellets (Carlo Erba Reagenti), chloroform (Aldrich).

High surface area graphite (HSAG) was Synthetic Graphite 8427® (Asbury Graphite Mills Inc.). Characterization of HSAG has been reported by some of the authors in previous works [49, 51,65,66]. Analyses have been repeated on the sample used for the present work, to confirm the reproducibility of what already published.

The Fourier-Transform Infrared (FT-IR) spectra were recorded in transmission mode (128 scan and 4 cm^{-1} resolution) in a diamond anvil cell (DAC) using a ThermoElectron Continuμm IR microscope coupled with a FT-IR Nicolet Nexus spectrometer.

PHI 5000 VersaProbe instrument (Physical Electronics) was used for survey scan and high resolution X-ray photoelectron spectroscopy (XPS). The powder was dried in oven at 100°C for 24 h at atmospheric pressure before analysis and thereafter placed in the XPS pre-chamber overnight, in order to avoid anomalous outgassing during the XPS characterization, performed in UHV condition (10^{-8} Pa). A monochromatic Al K-alpha X-ray source (1486.6 eV energy, 15 kV voltage and 1 mA anode current) and a power of 25.2 W were used for analysis. Different pass energy values were employed: 187.85 eV for survey spectra and 23.5 eV for high resolution peaks. Analyses were carried out with a take-off angle of 45° and with a 100 μm diameter X-ray spot size on a square area of 1400×1400 μm^2, with the aim to have a good average and better statistics of powder behavior. A double beam (electron and argon ion gun) neutralization system, dedicated to reduce the charging effect on samples, was also employed during data acquisition. All binding energies (B.E.) were referenced to the C1s line at 284.8 eV. Spectra were analyzed and peak deconvolution was performed using Multipak 9.6 software.

Raman spectra were recorded on powdered samples deposited on a glass slide by using an Horiba Jobin Yvon Labram HR800 dispersive Raman spectrometer equipped with Olympus BX41 microscope and a 50X objective. The excitation line at 632.8 nm of a He/Ne laser was kept at 0.5 mW in order to prevent samples degradation. The spectra were obtained as the average of four acquisitions (30 seconds each) with a spectral resolution of 2 cm^{-1}. The Raman spectra reported in this work are the average of spectra recorded in five different points of the samples.

Wide-angle X-ray diffraction (WAXD) patterns were obtained in reflection, with an automatic Bruker D8 Advance diffractometer, with nickel filtered Cu–Kα radiation. Patterns were recorded in 10° – 100° as the 2θ range, being 2θ the peak diffraction angle. Distance between crystallographic planes was calculated from the Bragg law. The $D_{hk\ell}$ correlation length, in the direction

perpendicular to the *hkl* crystal graphitic planes, was determined applying the Scherrer equation (equation (1)).

$$D_{hk\ell} = K\,\lambda / (\beta_{hk\ell} \cos\theta_{hk\ell}) \quad (1)$$

where: K is the Scherrer constant, λ is the wavelength of the irradiating beam (1.5419 Å, Cu-Kα), $\beta_{hk\ell}$ is the width at half height, and $\theta_{hk\ell}$ is the diffraction angle. The instrumental broadening, *b*, was determined by obtaining a WAXD pattern of a standard silicon powder 325 mesh (99%), under the same experimental conditions. The width at half height, $\beta_{hk\ell} = (B_{hk\ell} - b)$ was corrected for each observed reflection with $\beta_{hk\ell} < 1°$ by subtracting the instrumental broadening of the closest silicon reflection from the experimental width at half height, $B_{hk\ell}$.

~~*2.2 Preparation of polyhydroxylated graphene layers (G–OH)*~~

~~G–OH was prepared by reacting HSAG and KOH in a planetary ball mill S100 from Retsch, with 0.3 L grinding jar moving on a horizontal plane. The jar was loaded with 6 ceramic balls having a diameter of 20 mm. HSAG (1g), KOH powder (20 g) and H_2O (6.5 mL) were put into the jar, that was allowed to rotate at 300 rpm, at nominal room temperature, for 10 hours. After this time, the mixture was placed in a Büchner funnel with a sintered glass disc and repeatedly washed with distilled water (6 x 100 mL) under vacuum. Finally, the obtained solid was put in an oven to remove excess water. 1.1 g of black powder were obtained.~~

2.2 Reimer-Tiemann reaction performed at nominal room temperature (Procedure 1)

In a round bottomed flask equipped with magnetic stirrer and condenser, KOH powder (3.12 g, 55 mmol), $CHCl_3$ (1.12 mL, 14 mmol) and H_2O (0.5 mL) were added in sequence. G-OH (0.500 g) was added to such mixture after few seconds, to avoid chloroform decomposition by alkaline ions, well known problem in Reimer-Tiemann reaction performed on phenol ring. The mixture was stirred at room temperature, for 12 hours. After this time, solvent was removed at reduced pressure. The solid was reduced in fine grains in a mortar with a pestel, transferred into a Falcon™ tube (15mL) and water (10 mL) was added. The suspension was sonicated for 10 minutes and centrifuged at 4000 rpm for 10 minutes (3 times). 0.7 g of black powder were obtained.

2.3 Reimer-Tiemann reaction performed at nominal 0°C (Procedure 2).

The procedure reported in the previous paragraph was adopted also for the reaction performed at 0°C, keeping the round bottomed flask in an ice bath. 0.67 g of black powder were obtained.

2.4 Reimer-Tiemann reaction performed at nominal 0°C with sequential addition of $CHCl_3$ (Procedure 3)

In a round bottomed flask equipped with magnetic stirrer and condenser, KOH powder (3.12 g, 55 mmol), G-OH (0.5 g) and H_2O (0.5 mL) were added in sequence. $CHCl_3$ (1.12 mL, 14 mmol) was added to such mixture after few seconds in three parts (3 x 0.37 mL). The mixture was stirred at 0°C for 12 hours. After this time, solvent was removed at reduced pressure. The solid was reduced in fine grains in a mortar with a pestel, transferred into a Falcon™ tube (15mL) and water (10 mL) was added. The suspension was sonicated for 10 minutes and centrifuged at 4000 rpm for 10 minutes. This procedure was repeated three times. Byproduct such as KCl was extracted by water. 0.50 g of black powder were isolated. The pH was measured to be 14 immediately after the dispersion of KOH in the reaction medium and 13.8 shortly before the work-up.

2.5 Preparation of chitosan based nanocomposites

G-CHO (0.4 g) and chitosan (0.4 g) were mixed for 5 minutes in a mortar with the help of a pestle. The mixture was dispersed in water (8 mL) and 4 drops of an aqueous solution of acetic acid 99.7% (0.010 g, 9.9 10^{-3} mol) were added, obtaining a homogenous suspension. Acetic acid was used in such an amount to lead to the protonation of about 7% of chitosan amino groups.

The so obtained water suspension was sonicated for 15 minutes. Casting of G-CHO/CS suspension was performed on a glass plate in which an adhesive tape was used to delimit the area. Sheets were formed after water evaporation, at room temperature and at atmospheric pressure (24 hours).

3. Results and discussion

3.1 Preparation and characterization of graphene layers with oxygenated functional groups

Prior to functionalization, the graphitic sample used in this work (HSAG) was duly characterised. Chemical composition, determined by elemental analysis, was (mass %): carbon 99.5, hydrogen 0.4, nitrogen 0.1, oxygen 0.0. TGA revealed the following mass loss: 3.2% below 700°C. Surface area was determined by BET according to ASTM D6556 method and was found to be 330.3 m^2/g. Average size of HSAG particles was evaluated by means of dynamic light scattering [65], obtaining values representing the hydrodynamic radius of HSAG particles in water dispersions. Average values were 500 nm in the as prepared dispersion and 190 nm after centrifuging the dispersion for 30 min centrifugation at 9000 rpm. Transmission electron micrograph taken on supernatant suspension after 60 min centrifugation at 9000 rpm revealed graphite stacks randomly arranged,

with lateral size between about 300 nm and 500 nm [51]. FT-IR, XPS and Raman characterization showed that no oxygenated functional group was present prior functionalization (see below).

In the first step of the reaction pathway of Figure 1, the high surface area graphite (HSAG) was reacted with KOH, with the help of mechanical energy (through ball milling, details in [51]), obtaining G-OH. Elemental analysis confirmed the results already reported [51]. Elements other than carbon, oxygen, hydrogen and nitrogen were not found. The oxygen content was found to increase to about 6 mass%. A larger mass loss was found for G-OH, below 700° C, than for HSAG. Data are reported in [51]. XPS analysis, commented below in the text, revealed also the presence of potassium. Size of G-OH nanoparticles was evaluated by means of dynamic light scattering and High-Resolution Transmission Electron microscopy (HRTEM). As already reported [51], treatment of HSAG with KOH via ball milling led to the reduction of HSAG aggregates size: from about 190 nm (HSAG) to about 150 nm, for particles in supernatant suspensions (centrifugation at 9000 rpm for 60 min). TEM micrographs confirmed that the lateral size of HSAG and G-OH were of the same order of magnitude, in samples isolated after centrifugations [51]. These data suggest that the milling step does not cause appreciable breaking of the graphitic layers. Micrographs taken at higher magnification on graphene layers disposed perpendicularly to the beam allowed to visualize stacks with thickness of about 1.7 – 4.8 nm, hence with 6 to 15 stacked graphene layers. Stacks with low number of layers were frequently observed [51].

Reaction of G-OH with $CHCl_3$ was performed by adopting different procedures, described in detail in the experimental part. In a first approach (Procedure 1), KOH powder, $CHCl_3$ and H_2O were mixed and G-OH was added after few seconds, to avoid chloroform decomposition by alkaline ions, which is known to occur in the case of Reimer-Tiemann reaction performed on phenolic rings. The reaction was performed at 21°C (room temperature in the text) as usually done in the scientific literature [52,53]. An extraordinary reactivity was observed (see Figure S1 in Supplementary Material). To avoid such uncontrolled behaviour, the reaction was carried out at 0°C (Procedure 2). Moreover, G-OH, KOH powder and H_2O were mixed at 0°C and $CHCl_3$ was added in three different steps, in smaller portions (Procedure 3).

The characterization of the reactions products was performed by means of IR, XPS, Raman, WAXD spectroscopies. In the following text, products from the reaction carried out at room temperature (Procedure 1) and at 0°C with the successive addition of small $CHCl_3$ portions (Procedure 3) are described. They are labelled G-COOH and G-CHO, respectively. Product from Procedure 2 is described in the Supplementary Material.

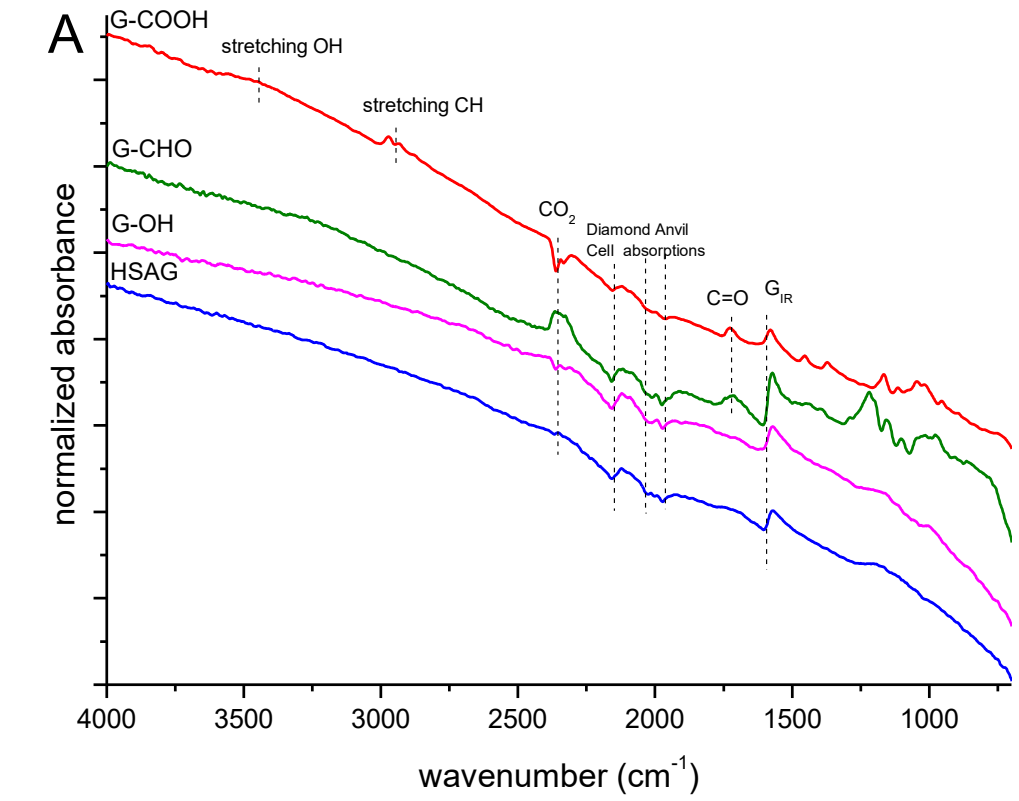

250

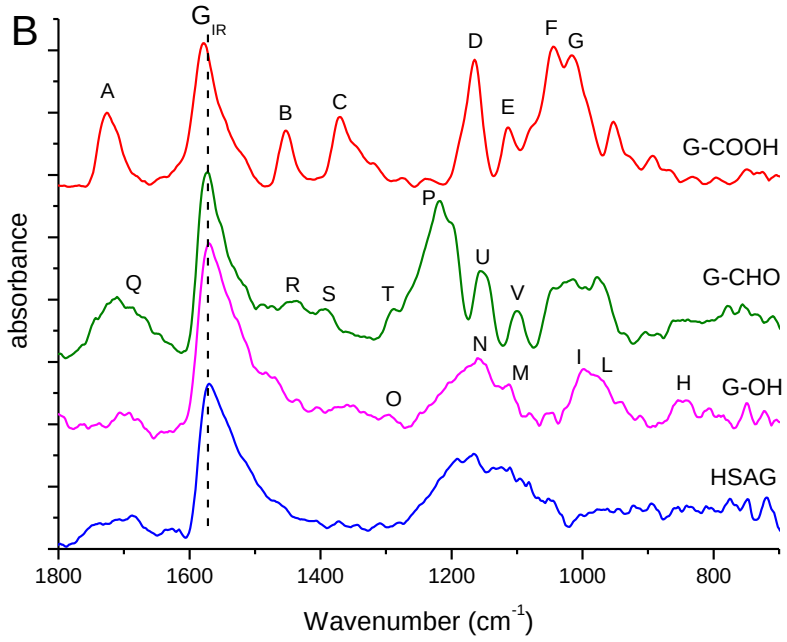

251

252 **Figure 2.** FT-IR spectra of HSAG (blue), G-OH (purple), G-CHO (green) and G-COOH (red): in
253 the full region 4000-700 cm^{-1} (A) and zoom in the region 1800-700 cm^{-1} (B). Spectra are displayed
254 after baseline correction.

255

In Figure 2A and 2B the IR spectra of the materials under investigation are reported. As explained in detail in the experimental part, IR spectra have been recorded in transmission using a diamond anvil cell (and not in KBr pellet) in order to avoid the presence of the absorption features due to the water molecules that are typically absorbed by KBr during sample preparation. Spectra were obtained from the absorption of very thin films of HSAG particles, which are not transparent to the IR beam. Indeed, the $\mathbf{G_{ir}}$ absorption observed in the spectra at 1590 cm^{-1} is mostly due to the reflection from the graphitic planes as revealed by its shape, which resembles a sigmoid function (as expected in specular reflection IR spectroscopy). The strong light diffusion from the HSAG particles is responsible for the increase of the spectra toward high wavenumbers. Details about the interpretation of the signals coming from HSAG and G-OH can be found in previous publications [51,65,66]. Some comments are also reported in this paper to allow direct comparison. The spectrum of the product of the reaction performed at room temperature between $CHCl_3$/KOH and G-OH (G-COOH) reveals a variety of strong and structured bands, which can be assigned to vibrations of different oxygenated functional groups. It is worth reminding that this family of functional groups show, in IR spectra, the Lorentzian and/or Gaussian profile of an absorption phenomenon. Such profile is observed also in the spectrum of G-CHO in Figure 2. Bands due to G-CHO in Figure 2 appear very different with respect to the signals present in IR spectra of GO or reduced GO. Due to the complexity of the systems, the proposed assignment of the peaks is based on correlative spectroscopy [67]. In Figure 2A the broad and weak absorption at 3400 cm^{-1} can be assigned to -OH stretching vibrations of hydrogen bonded hydroxy groups already present in G-OH. At 1590 cm^{-1} the signal common to all the samples is assigned to the E_{1u} IR active mode of the collective C=C stretching vibration (G_{IR}) of graphitic materials enhanced for the structural disordered and/or chemically functionalization of the graphitic layers. In the spectrum of G-COOH bands at 2967 cm^{-1}, 2928 cm^{-1} and 2874 cm^{-1} (absent both in HSAG and GOH) can be assigned to the CH stretching vibrations of CH_3 and CH_2 units. Therefore they can be associated to the presence of -CH_2-OH functional groups (i.e. benzylic alcohol moiety, absent in the spectrum of G-OH).

In Figure 2B the spectrum of G-COOH shows a structured band at 1730 cm^{-1} (A) that can be assigned to -C=O stretching vibration of -COOR functionalities (acid and/or ester). The frequency of the stretching of this vibration is compatible with the possible formation of intramolecular hydrogen bonds between -C=O and -OH groups which are close to each other in aromatic compounds such as salicylic acid and its derivatives. The band at 1450 cm^{-1} (B) can be assigned to bending vibrations of CH_2 and CH_3 groups and the broad and asymmetric band at 1371 cm^{-1} (C) to both the CH_3 symmetric bending and the out of plane vibration of -OH groups. The strong bands at

1164 cm^{-1} (D), 1111 cm^{-1} (E), 1042 cm^{-1} (F), and 1014 cm^{-1} (G) can be assigned to the stretching vibrations of C-O-C and C-OH functional groups.

In the spectrum of G-OH bands at 846 cm^{-1} (H) and 1000 cm^{-1} (I) can be assigned to vibrations of aryl-OH groups, and bands at 975 cm^{-1} (L), 1121 cm^{-1} (M), 1158 cm^{-1} (N), and 1290 cm^{-1} (O) are compatible with vibration of epoxy or ether groups.

The spectrum of G-CHO (i.e. the product of the reaction performed at 0°C with successive additions of small $CHCl_3$ portions) shows many features observed also for G-OH. A relevant difference is the presence of the strong band at 1220 cm^{-1} (P), and the broad and structured band at 1715 cm^{-1} (Q) which can be assigned to -C=O stretching vibration of aldehydic functionalities. Other bands at 1438 cm^{-1} (R), 1390 cm^{-1} (S), 1290 cm^{-1} (T), 1158 cm^{-1} (U), and 1100 cm^{-1} (V) have a good correspondence with the absorptions of benzaldehyde and salicylaldheyde [68] molecules.

The IR spectroscopic evidences indicate that the reaction between G-OH and $CHCl_3$/KOH introduces new functional groups onto the graphene layers. The type of functional groups introduced depend on reactions conditions: -OH, -COOR (acid and/or ester) and -CH_2-OH groups were introduced when the reaction was performed at room temperature and reagents were added in one shot. When the reaction was carried out in milder conditions, at 0°C with successive $CHCl_3$ additions, aldehydic groups were selectively formed. This latter procedure (Procedure 3) seems thus to allow the selective occurring of Reimer-Tiemann reaction. Domino reaction made by Reimer-Tiemann followed by Cannizzaro disproportionation appears instead to occur when the high surface area graphite reacts with KOH/$CHCl_3$.

XPS spectra of HSAG, G-OH, G-CHO and G-COOH are shown in Figure 3. The main signals of all the samples are due to C_{1s} and O_{1s}. In the case of HSAG, as discussed in [51], a surface oxidation was detected (O_{1s}/C_{1s}=0.04, 4.2% atomic) while elemental analysis did not reveal the presence of oxygen. G-OH presented however a larger amount of oxygen: O_{1s}/C_{1s}=0.07, 6.4% atomic.

In the XPS wide scan spectrum of G-COOH, besides the two main signals, C_{1s} at B.E.=284.8 eV and O_{1s} at B.E.=533.0 eV, presence of K and Cl is also revealed. The O_{1s}/C_{1s} atomic ratio has a value of 0.09, which is higher than the ratio estimated in G-OH (0.07); the oxygen content is 8.2% atomic. The G-CHO sample presents an oxygen content of 10 % atomic and O_{1s}/C_{1s}=0.12.

By the C_{1s} peak deconvolution, three components were detected (see Figure S2 and Table S1 in Supplementary Material). One peak has the same position as that of graphite (284.8 eV), with the characteristic tailing on the high energy side, due to the π bond shake-up satellite, which are clear in the HSAG spectrum [51]. The other two components of C_{1s} are found at higher binding energies, due to the electron withdrawing effect of oxygen. They are attributable to **C**-O and **C**=O functions. The C=O/C-O ratio is 0.45 for HSAG, decreases to 0.18 and 0.16 for G-OH and G-COOH

respectively. Interestingly the value is 0.55 for G-CHO and this indicates that carbonyl functions are the prevailing ones among the oxidized groups.

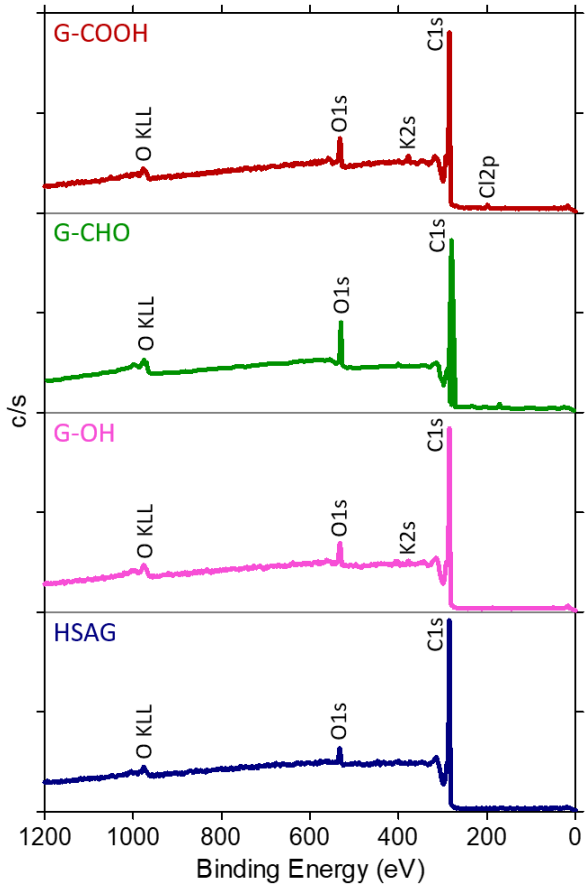

Figure 3. Wide scan XPS spectra of HSAG, G-OH, G-CHO and G-COOH.

To better understand the nature of the oxidized groups, a narrow scan on the O_{1s} peak and its deconvolution was performed (see Figure S3 in Supplementary Material). In fact, analysis of the C_{1s} spectrum does not allow accurate characterization, due to the large contribution of C sp^2, which tends to mask relative contributions of other groups [69]. Information provided by the analysis of the O_{1s} can therefore better complement the information gathered by the IR spectra. It has however to be taken into account that XPS analysis probes only the outer layer (about 40 Å thick) of the graphitic material and the O_{1s} spectra can be more surface specific than C_{1s} spectra.

For G-COOH as for G-OH, there are two main contributions to O_{1s} signal, i.e., at 531.3 eV and 533.2 eV, a minor component at 535.2 eV and a negligible signal at 530.4 eV. The main components are located at slightly different energies than G-OH. On the basis of the literature data, one can attribute the signal at 531.3 eV to C=**O** groups of carbonyl and carboxyl groups (they count for around 50% of the signal intensity) with a shift of 0.2 eV with respect to G-OH. The component

at 533.2 eV (again 0.3 eV shifted with respect to G-OH) evidences the presence of C-**O** groups identified as hydroxyl and ether groups bonded to aromatics. The contribution could account for both phenolic and benzylic OH, but they cannot be separately identified. The minor component at higher binding energy can be attributed to adsorbed water and oxygen.

In G-CHO, three components appear by deconvoluting the O_{1s} signal: a negligible peak at 530.2 eV and two main components of similar intensity at 531.5 and 532.9 eV. They could be interpreted as signals due to C=**O** groups and C-**O** groups as in G-COOH. However the second peak appears at a lower binding energy (532.9 instead of 533.2 eV): it can account for aliphatic C-**O** but it could also be a shake-up feature from the C=**O** peak [70].

Both IR and XPS findings indicate the formation of aldehydic derivatives of G-OH, G-CHO, after the reaction with $CHCl_3$/KOH at 0°C through Procedure 3. Further oxidized species detected by XPS appear to be confined in an outer layer. A different product, G-COOH, is obtained, allowing the occurring of disproportionation Cannizzaro reaction.

To demonstrate that the functionalization of the graphene layers does not modify the crystalline structure, Raman spectroscopy analysis was performed on HSAG, G-OH and G-COOH and spectra are shown in Figure 4.

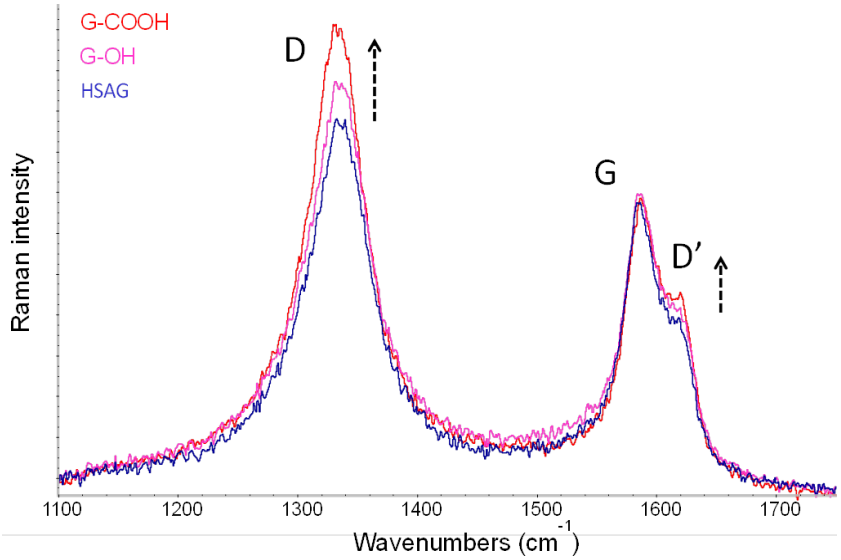

Figure 4. Raman spectra of HSAG (red), G-OH (blue) and G-COOH (purple) excited at 632.8 nm.

All spectra show a similar pattern with the G band at 1582 cm^{-1} and evident D and D' bands at 1333 cm^{-1} and 1620 cm^{-1} respectively. The G peak is assigned to the E_{2g} Raman active mode of collective C=C stretching vibration of crystalline graphite (graphene), whereas the D and D' peaks appear when structural defects, such as holes, sp^3 or sp carbon atoms, dangling bonds, distortions from planarity, grafted functional groups or confinement (e.g. by edges), affect the graphitic layers. Finite

dimensions of the graphitic platelets lead to larger amount of irregular boundaries and, as a consequence, to larger intensity of D and D' peaks [51]. HSAG consists of platelets with a surface of approximately 500 x 500 nm^2. Such low size can be attributed to the production via ball milling, which cracks the layers, however without substantially altering the in plane order, as revealed by X-ray analysis. The in plane order was maintained also after ball milling with KOH and after the chemical reactions. The enhancement of D band in the spectrum of G-OH can be thus assigned to the hydroxyl functionalization of graphene edges. A further enhancement of D and D' peaks are observed for G-COOH as consequence of the introduction of additional functional groups after reactions of G-OH with $CHCl_3$/KOH, while indeed new Raman components between G and D peaks, due to disordered sp^3 carbon structures, are not appreciable [71]. One can conclude that the bulk structure of the graphitic layers is essentially unaffected by the functionalization reaction.

The essentially unaltered in plane order and interlayer distance allow to assume that functionalization occurred on peripheral positions, reasonably mainly on sites located around the borders of the platelets. This is consistent with the observed stability of the G peak which does not change either the intensity or the frequency. Frequency shifts of the G peak in graphene or the appearance in graphite of a second component at higher Raman shifts are observed for doped graphene, [72-75] and graphite intercalation compounds [72-76].

The inspection of Raman spectra leads to exclude the presence of species intercalated between the graphene layers, because their occurrence should generate frequency shifts and/or a second component of the G peak, as normally observed for intercalated Graphite Intercalation Compounds GICs [72-74]. The intercalation of chemical species in between graphene layers is indeed a relevant aspect to be investigated, when graphene layers undergo chemical reactions. Chemical substances could also be absorbed on the carbon material. As discussed in the next paragraph, the presence of absorbed molecule was also investigated and excluded by performing *ad hoc* experiments.

The WAXD pattern in Figure 5 reveals that the (002) reflection of G-OH (Figure 5b) and G-COOH after purification (Figure 5d) are at the same 2θ value as in the pristine HSAG sample (Figure 5a). A number of about 22 stacked layers in G-OH (about 35 were in HSAG [51]) was estimated by applying the Scherrer equation. The presence of 100 and 110 reflections, with intensity similar to the one in pristine HSAG, indicates that G-OH and G-COOH remain substantially unaltered: they are thus formed by a low number of stacked graphene layers, the core of which has the ideal graphitic structure. Interestingly, the WAXD profile of G-COOH before purification (Figure 5c) is different: it shows peaks at 28.5 (200), 40.7 (220), 49.9 (222), 58.6 (400), 66.5 (420), 73.7 (422), which can be attributed to KCl. It can be assumed that KCl promotes the exfoliation of the material. In fact, the preparation of exfoliated graphite from hydrothermally synthesized graphite-KCl

compounds has been reported [78]. The removal of KCl by the purification procedure (see experimental part) can restore the stacking of graphene layers. WAXD patterns, in particular the (002) reflection at the same 2θ value in HSAG and in the functionalized samples, lead to exclude the presence of intercalated compounds [79].

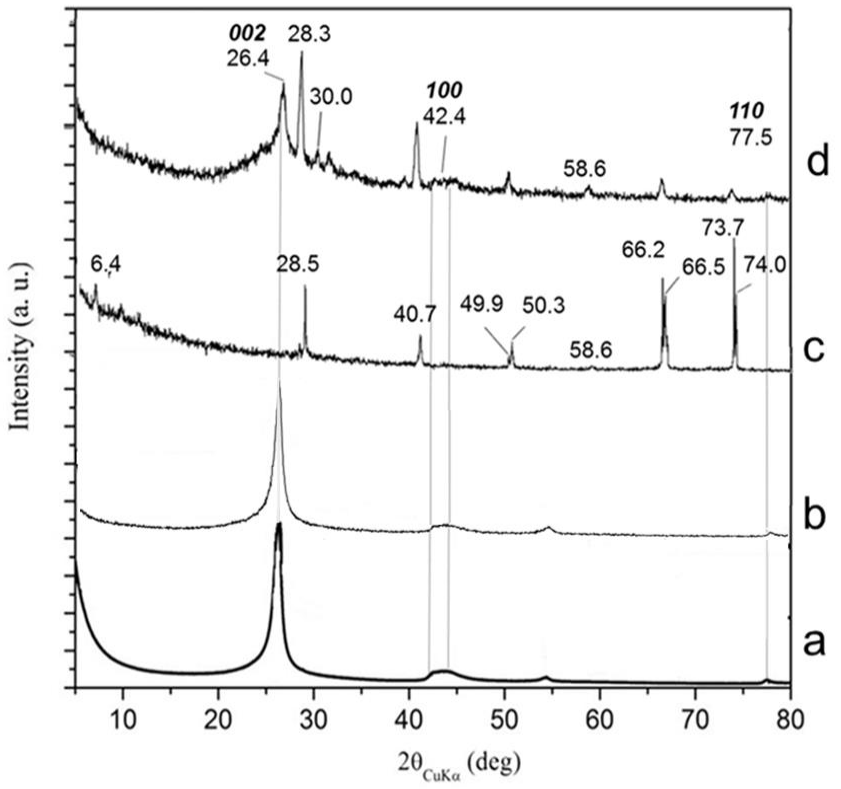

Figure 5. WAXD patterns of HSAG (a), G-OH (b), G-COOH before purification (c) and after purification (d).

Experimental findings discussed so far indicate that the reactions proposed in this work (Figure 1) preserve the bulk structure of graphene layers through all the processes.

3.2 Mechanisms proposed for the functionalization reactions of graphene layers

Experimental findings reported above reveal that the reaction of polyhydroxylated graphene layers with $CHCl_3$/KOH/H_2O led to the modification of graphene layers with oxygenated functional groups.

Results from analytical investigations allow to identify the nature of the functional groups: aldehydic groups were observed when the reaction was performed at 0°C and benzyl alcohol and carboxy groups (prevailingly ester) when the reaction was carried out at nominal room temperature.

Below in the text, it is shown the formation of imines from the reaction of G-CHO with chitosan. This appears a support of the presence of aldehydic groups on the graphene layers.

The presence of intercalated oxygenated species can be ruled out on the basis of Raman and WAXD results. As anticipated above, the presence of low molar mass oxygenated molecules only absorbed on the graphene layers was also investigated. G-OH was mixed with an excess of formaldehyde (even though it would be hard to justify the presence of formaldehyde) for 12 hours and FT-IR spectrum was immediately recorded, without observing any modification (Supplementary Material S1).

In order to elaborate an interpretation of the results so far reported, the scientific literature has to be carefully considered. For example, it was reported that by using the same reaction mixture, $CHCl_3$ in alkaline medium, in the presence of a phase transfer catalyst, cyclopropanation reaction occurs on alkenylic substrates [56] and at the edges of graphene layers [55]. These reagents are not the preferred ones for cyclopropanation, as cyclopropanes are traditionally formed by adding the methylene–zinc–iodide complex, generated from diethyl zinc and diiodomethane [57,58,79], or by transition metal-catalyzed decomposition of diazo compounds [59]. Moreover, cyclopropanation reaction was reported [55] to occur on the graphene layers in the presence of a phase transfer catalyst, which was not used in the work here reported. However, to investigate and, in case, to rule out the formation of cyclopropane ring, pristine HSAG was mixed with KOH powder, $CHCl_3$ and H_2O. Results of this experiment are reported as Supplementary Material S2. Infrared spectrum is shown in Figure S5. Typical spectral features of cyclopropane rings cannot be detected, confirming that the phase transfer catalyst, as reported in literature [56], is needed.

In the light of what discussed so far, the following mechanism can be proposed. The functionalization of graphene layers occurred through Riemer-Tiemann reaction (introduction of aldehyidic groups) and domino Reimer-Tiemann / Cannizzaro reaction (benzyl alcohol and carboxy groups). The mechanism for these reactions is presented in Figure S6 of the Supplementary Material and discussed in the following.

~~**Figure 6.** Proposed synthetic pathway for the reaction of G-OH with $CHCl_3$/KOH at room temperature: mechanism of Reimer-Tiemann (A) and Cannizzaro (B) reactions.~~

Figure S6A shows the mechanism for the introduction on graphene layers of aldehyde functional groups, through the Reimer-Tiemann reaction. It is known that chloroform reacts with aqueous potassium phenoxide very slowly at room temperature, but its reactivity remarkably increases in the presence of a strong base such as KOH [54]. KOH deprotonates $CHCl_3$, leading to a trichlorocarbanion, and deprotonates the OH groups on the graphene layer as well, forming product **1**. The trichlorocarbanion, through a quick α-elimination, spontaneously loses a chloride ion

forming neutral dichlorocarbene, the reactive species that attacks **1**. The negatively charged phenoxide-like rings in **1**, with their negative charge delocalized on many aromatic rings, have a large resonance stabilization. Dichlorocarbene could react with both the phenoxide ion and the carbon atoms in the ortho positions with respect to the oxygenated group. Indeed, both mechanisms are reported in scientific literature [54]. Reactivity with ortho positions is favored by the charge delocalization which increases nucleophilicity of the carbon atoms. As a matter of fact, only this reactivity can account for the formation of an aldehydic species. Moreover, studies on the reactivity of dichlorocarbene in the Reimer-Tiemann reaction [54] demonstrated the quick formation of o- and p-hydroxybenzaldehydes. FT-IR findings suggested that dichlorocarbene attacks carbon atoms in ortho position with respect to aldehyde. Hence, dichlorocarbene gives rise to an attack on the ortho carbon atom of the phenoxide ion, forming product **3**, through the dichloro intermediate **2**. Such regioselective ortho attack, followed by 1,2-proton transfer, is the preferred mechanism [54], even though the intermolecular proton transfer mediated by water cannot be ruled out. Hydrolysis promoted by KOH leads to o-hydroxyformyl graphene layers, i.e. final product **6**, with CHO group in ortho position with respect to OH.

This mechanism suggests that oxygenated functional groups are located on the edges of the graphene layers and that a reaction occurs on graphene layers in the armchair configuration, which have two neighboring reactive sites. The Reimer-Tiemann reaction leads to the formation, for each CHO mole, of three KCl moles, which indeed affect the organization of graphene layers, favoring their impressive exfoliation [29], as shown by WAXD results (Figure 5). The functionalization degree of this reaction is reported in the Supplementary Material S3.

Figure S6B of the Supplementary Material shows the mechanism for the Cannizzaro disproportionation reaction, which occurs at room temperature and leads to the introduction of benzyl alcohols and carboxy functional groups on graphene layers. Product **6**, obtained through a Riemer-Tiemann reaction, undergoes a nucleophilic attack of the hydroxide ion on the aldehydic group. The tetrahedral carbon (intermediate **7**) expels a hydride ion becoming a potassium carboxylate group (product **8**). A second molecule of o-hydroxyformyl graphene **6** undergoes a nucleophilic acyl addition by the hydride ion. The benzyloxy intermediate **9** becomes alcohol (**10**) upon washing with water. Therefore, the Cannizzaro reaction can only occur on aldehydes lacking hydrogen atoms in the α positions. In fact, aromatic substrates with α hydrogens undergo instead deprotonation leading to enolates: these species are not detected in the IR spectra of isolated products. Carboxy functional groups could be due to both acids and esters. The presence of esters could be justified if we hypothesize the condensation of benzyl alcohol and acid groups. Indeed, the Cannizzaro reaction is used on an industrial scale for the preparation of esters starting from

aldehydes. In order to estimate to what extent esterification reaction occurred, calculations (reported as Supplementary Material S4) have been attempted. They seem to indicate that esterification reaction may occur. Graphene layers with alcohol and acid functional groups could be then be prepared through hydrolysis.

The efficiency of the domino process, documented in Figure S1 (Supplementary Material), can be explained taking into account that both Reimer-Tiemann and Cannizzaro are exothermic reactions, in particular the former one. In spite of such efficiency, the bulk structure of graphene layers was substantially unaltered and this is in line with functionalization on peripheral positions. In the Supplementary Material S5, it is reported the characterization of graphene layers obtained from the reaction of G-OH with $KOH/H_2O/CHCl_3$ at 0°C (Procedure 2). It is worth summarizing that disproportionation reaction was not prevented: indeed, aldehydes were detected together with carboxylic acids.

It is definitely important pondering why G-OH allows the occurring of the domino reaction. Only speculations can be attempted. Two key steps characterize Cannizzaro disproportionation: (i) the formation of the carboxy group with the expulsion of a hydride ion, (ii) the addition of the hydride ion to a second mole of aldehyde. The carboxy group in G-OH could have high stability thanks to the conjugation allowed by an infinite polycyclic aromatic hydrocarbon such as graphene. Such stability allows an easy leaving of the hydride ion, which could be adsorbed on the graphene layer, as potassium salt. Indeed, the absorption on graphene of hydrides of electropositive metals is studied as tool for hydrogen storage [80]. Moreover, it could also be hypothesized that electron rich G-OH adsorbs the reagents, acting as a catalyst for oxidation promoted by the oxygen dissolved in the alkaline medium.

According to the reported mechanisms, the functionalization should occur on the edges of the graphene layers. This could account for the difference of the IR spectra of the present work with respect to the IR spectra of GO or reduced GO, where functional groups are expected over the entire graphene plane. Moreover, Cannizzaro disproportionation reaction is known to occur moving from aldehydes in the absence of acidic hydrogen on the alpha carbons, as it would be G-CHO. It is not the purpose of this work to stretch inferences too far. However, a good number of experimental data and analytical indications seem to support the plausibility of the above reported mechanisms. More than that, they indicate that graphene layers were chemically modified with oxygenated functional groups.

3.3 Nanocomposites based on G-CHO and chitosan

With the aim to prove a viable use of functionalized graphene layers, exploiting the aldehydic groups, bionanocomposites were prepared based on G-CHO and chitosan. The objective was to crosslink chitosan with the graphene layers, thanks to the reaction between aldehydes and amino groups. It is well known that chitosan can be crosslinked by dialdehydes and a molecule such as glutaraldehyde is traditionally used [81], in spite of its critical aspects as for the impact on human health. In the scientific literature, nanocomposites based on chitosan and graphene related materials (i.e., graphene oxide or reduced graphene oxide) have been reported for different applications, such as the preparation of highly compatible membranes [82], the detection of human epidermal growth [83] and bone tissue engineering [84]. Improved properties are expected for the bionanocomposite based on chitosan and G-CHO, thanks to the unperturbed nature of the graphene layers. To verify the feasibility of the crosslinking reaction of G-CHO with amino groups, hexamethylenediamine was successfully used as the crosslinking agent. Results are reported as Supplementary Material S6. In this manuscript, reaction of G-CHO with chitosan and main materials molecular features are reported, while the assessment of its physico-mechanical properties will be the focus of a future work.

Reaction between G-CHO and CS was performed as described in the experimental part and schematically shown in Figure 6.

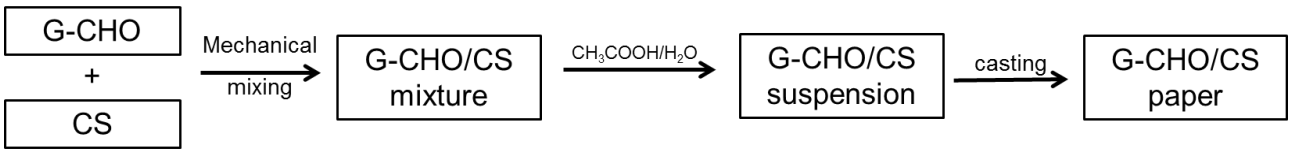

Figure 6. Block diagram for the preparation of G-CHO/CS paper.

In brief, G-CHO and CS were first premixed in a mortar with the help of a pestle. Water dispersion of the formed adduct was prepared in the presence of acetic acid. These dispersions were stable for at least 1 week. Flexible carbon paper (Figure 7a) was then prepared by simply casting the dispersion on a glass support and waiting for water evaporation. Characterization of G-CHO/CS carbon paper was performed by means of FT-IR (Figure 7b) and XPS (Figure 7c and 7d).

In Figure 7b, spectra of solid CS, G-CHO/CS paper and G-CHO are reported in the region 1800 – 800 cm^{-1}. In the spectrum of pure CS (A) the strong and structured band at 1558 cm^{-1} with a shoulder at 1575 cm^{-1} could be assigned to the overlap of the -CN- stretching (amide II) of the $C{=}ONHCH_3$ group (chitin units) and of the $-NH_2$ bending vibration of the primary amine (deacetylated chitin units). The sharp peak at 1378 cm^{-1} is assigned to the symmetric bending of

552 methyl groups (“umbrella” motion of chitin groups). The four strong and sharp peaks in the region
553 1200 cm^{-1} - 1000 cm^{-1} could be assigned to CO stretching modes of –COH, -COC- and –CH_2OH
554 groups of the glycosidic ring [85]. The occurrence of sharp and well-defined absorption bands and
555 of the doublet at 1659 cm^{-1} and 1625 cm^{-1} (assigned to NH bending in crystalline α-chitin) suggests
556 the presence in the solid of crystalline domains.
557 In the spectrum of the G-CHO/CS paper (B) the G_{IR} peak at 1590 cm^{-1} and the main absorption of
558 CS can be observed. However, all the absorption bands are broader; there is a peak shift and band
559 overlapping. This observation supports the occurrence of structural disorder CS moiety in the
560 carbon paper. Interestingly the well-defined band at 1715 cm^{-1} (observed in the spectrum of G-CHO
561 and assigned to -C=O stretching vibration of aldehydic functionalities) is strongly reduced in
562 intensity while a new medium-weak feature at 1656 cm^{-1} appears. Although in this region features
563 due to ammidic functionalities of CS are expected, the contemporary presence of the band at 1656
564 cm^{-1} associated to the strong -C=O stretching reduction highly support the formation of imine
565 groups between CS and G-CHO.
566 The wide scan XPS spectrum of G-CHO/CS carbon paper contains signals from C1s, O1s and N1s,
567 as expected; minor amounts of Na, Si and Ca are present. Deconvolution was attempted for carbon
568 and nitrogen signals, although it is difficult to precisely assign the individual contribution of the
569 several groups in both the C_{1s} and N_{1s} peak. The N_{1s} narrow scan signal (Figure 7c) presents one
570 component at 399.6 eV: it can account for amine and amide belonging to chitosan (partially
571 deacetylized), imine, imide, amide groups resulting from a reaction between chitosan and the
572 oxygen containing groups of the carbon material. Therefore the presence of C-N and C=N groups
573 due to a covalent attachment of the macromolecule to the functionalized graphene can be predicted.
574 The deconvolution of the C_{1s} peak results in three components (Figure 7d). The one at 284.7 eV
575 corresponds to sp^3 carbon and can also be assigned to **C**-N groups which have been formed by the
576 already commented direct reaction of the polyamines with the C=C double bonds of the carbon
577 material. The component at 286.2 eV can be assigned to imine groups (**C**=N) and **C**-O. Other
578 carbon-nitrogen and C=O groups cause the component at 288.1 eV. These data can suggest the
579 covalent bonding of G-CHO and the amino groups of chitosan, namely the imino groups coming
580 from the reaction of the carbonyl functions introduced by the Riemer-Tieman functionalization.
581 Comparing the C_{1s} narrow scan XPS spectra of G-CHO/CS carbon paper to those collected on
582 chitosan mixed with HSAG [65], binding energy shifts are observed, which can further prove the
583 covalent linking.

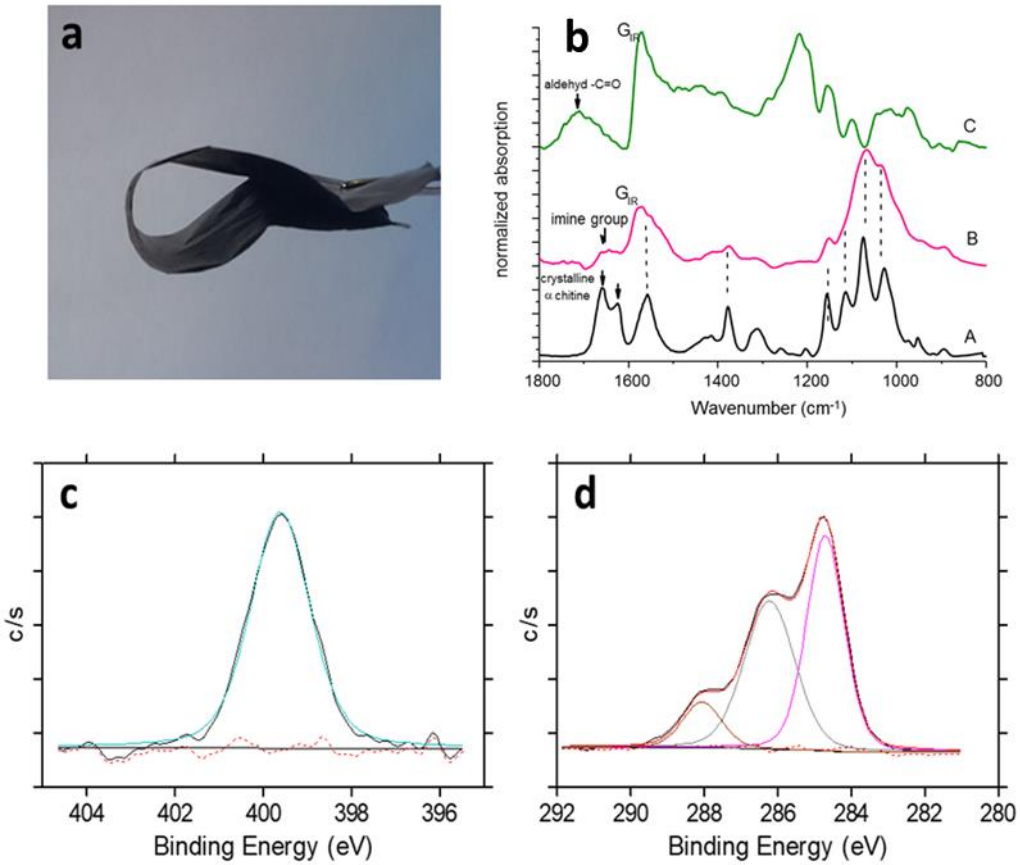

Figure 7. (a) Image of the flexible G-CHO/CS carbon paper; (b) FT-IR spectra of CS (A), G-CHO/CS carbon paper (B) and C-CHO (C) in the region 1900-700 cm^{-1}; (c) and (d) XPS narrow scans and peak deconvolution of N_{1s} (c) and C_{1s} (d) signals of G-CHO/CS carbon paper.

4. Conclusions

Polyhydroxylated graphene layers ~~were~~ reacted with KOH/H_2O and $CHCl_3$. When the reaction was performed at 0°C and $CHCl_3$ was added sequentially in small portions, aldehydic groups were detected on the graphene layers, as revealed by FT-IR spectra, XPS analysis and by the formation of imine functional groups after the reaction with the primary amines of chitosan. The presence of aldehydic functional groups can be justified ~~with~~ by the occurring of Reimer-Tiemann reaction, which is well known to happen to phenolic substrates reacted with $CHCl_3$ in alkaline medium. When the reaction was performed ~~done~~ at room temperature, benzyl alcohol and carboxy (prevailingly ester) groups were detected on the graphene layers. The Cannizzaro disproportion~~ation~~ reaction is known to lead to such functional groups moving from aldehydes in the absence of acidic hydrogen on the alpha carbons and could thus occur on the polyhydroxylated graphene layers that underwent Reimer-Tiemann reaction. Therefore it can ~~It could~~ be ~~thus~~ assumed that domino Reimer-Tiemann / Cannizzaro reaction occurred.

Graphene layers were thus functionalized with oxygenated functional groups. According to the reaction mechanism proposed, functionalization occured on the edges of the layers.

First proof of concept for a ~~first~~ viable usage of the produced graphene layers bearing aldehydic groups was the crosslinking of chitosan, with the preparation of stable water dispersions and flexible carbon papers, without using graphene oxide or reduced graphene oxide. Graphene layers act as crosslinker for chitosan and ingredient to give ~~for giving~~ mechanical resistance, electrical and thermal conductivities to the composite material. Future objectives of the research are to characterize and fully exploit such properties.

Acknowledgements

Prof. Attilio Citterio (Politecnico di Milano) is acknowledged for useful discussions. Authors gratefully acknowledge Dr Mario Maggio (Università degli Studi di Salerno) for the help with X-ray experiments. Financial support was from Fondazione Silvio Tronchetti Provera.

References

[1]. Novoselov, K. *et al*. Electric field effect in atomically thin carbon films. *Science* **306**,666–669 (2004).

[2]. Geim, A. K., MacDonald, A. H. Graphene: Exploring Carbon Flatland. *Phys. Today* **60**, 35-42 (2007).

[3]. Service, R. F. Carbon sheets an atom thick give rise to graphene dreams. *Science*, **324**, 875 (2009).

[4]. Novoselov, K. S., Geim, A. K., Morozov, S. V., Jiang, D., Katsnelson, M. I., Grigorieva, I. V., Dubonos, S. V., Firsov, A. A. Two-dimensional gas of massless Dirac fermions in graphene. *Nature* **438** (7065): 197-200 (2005).

[5]. Stoller, M. D., Park, S., Zhu, Y., An, J., Ruoff, R. S. Graphene-based ultracapacitors. *Nano Lett.* **8**: 3498-3502 (2008).

[6]. Chen, S., Wu, Q., Mishra, C., Kang, J., Zhang, H., Cho, K., Cai, W., Balandin, A. A., Ruoff, R. S. Thermal conductivity of isotopically modified graphene. *Nat. Mater.* **11**: 203-207 (2012).

[7]. Soldano, C., Mahmood, A., Dujardin, E. Production, properties and potential of graphene. *Carbon* **48**: 2127 –2150 (2010).

[8]. Ambrosi, A., Pumera, M., 2016. Electrochemically exfoliated graphene and graphene oxide for energy storage and electrochemistry applications. Chemistry-A Eur. J. 22, 153-159

[9]. Chua, C.K., Pumera, M., 2016. Facile labelling of graphene oxide for superior capacitive energy storage and fluorescence applications. Phys. Chem. Chem. Phys.18, 9673-9681.

[10]. Pushparaj V. L.; Shaijumon M. M.; Kumar A.; Murugesan S.; Ci L.; Vajtai R; Linhardt R. J.; Nalamasu O.; Ajayan P. M. Flexible energy storage devices based on nanocomposite paper. *Proc Natl Acad Sci USA* **2007**, 104, 34, 13574–7.

[11]. M. M. Waje, X. Wang, W. Li, Y. Yan. *Nanotechnology* **16** (7), 395 (2005)

[12]. Grennberg, H., Jansson, U. Synthesis of Graphene and Derivatives. *Science and Technology of Atomic, Molecular, Condensed Matter & Biological Systems* **2**: 105–127 (2012).

[13]. Hernandez, Y., Pang, S., Feng, X., Müllen, K. Graphene and Its Synthesis. *Polymer Science: A Comprehensive Reference* **8**: 415-438 (2012).

[14]. Eigler, S., Grimm, S., Hof, F., Hirsch, A. Graphene oxide: a stable carbon framework for functionalization. *J. Mater. Chem. A* **1**: 11559-11562 (2013).

[15]. Randviir, E. P., Brownson, D. A. C., Banks, C. E. A decade of graphene research: production, applications and outlook. *Mater. Today* **17** (9): 426-432 (2014).

[16]. Yang, H., Li, F., Shan, C., Han, D., Zhang, Q., Niu, L., Ivaskab, A. Covalent functionalization of chemically converted graphene sheets via silane and its reinforcement. J. *Mater. Chem.* **19**: 4632–4638 (2009).

[17]. Swager, T. M. Functional Graphene: Top-Down Chemistry of the π-Surface. *ACS Macro Lett.* **1**: 3−5 (2012).

[18]. Zaman, I., Kuan, H.-C., Meng, Q., Michelmore, A., Kawashima, N., Pitt, T., Zhang, L., Gouda, S., Luong, L., Ma, J. A Facile Approach to Chemically Modified Graphene and its Polymer Nanocomposites. *Adv. Funct. Mater*. **22** (13): 2735–2743 (2012).

[19]. Chua, C. K., Pumera, M. Covalent chemistry on graphene. *Chem. Soc. Rev.* **42:** 3222-3233 (2013).

[20]. Bhattacharjya, D., Jeon, I.Y., Park, H.Y., Panja, T., Beom Baek, J., Yu J.S., Graphene Nanoplatelets with Selectively Functionalized Edges as Electrode Material for Electrochemical Energy Storage. *Langmuir*, **31**, 5676−5683 (2015).

[21]. Xiong, P., Zhu, J., Zhang, L., Wang, X., Recent advances in graphene-based hybrid nanostructures for electrochemical energy storage. *Nanoscale Horiz*., **1**, 340—374 (2016).

[22]. Kausar, A., Anwar, Z., Khan, L. A., Muhammad, B., Functional graphene nanoplatelet reinforced epoxy resin and polystyrene-based block copolymer nanocomposite, *Fullerenes nanotubes and carbon nanostructures*, vol. 25, no. 1, 47–57 (2017).

[23]. Tan, Y.-Z., Yang, B., Parvez, K., Narita, A., Osella, S., Beljonne, D., Feng, X., Mullen, K., Atomically precise edge chlorination of nanographenes and its application in graphene nanoribbons, *Nat. Commun*., **4**, 2646 (2013).

[24]. Xu, J., Jeon, I.-Y., Seo, J.-M., Dou, S., Dai, L., Baek, J.-B., Edge-Selectively Halogenated Graphene Nanoplatelets (XGnPs, X= Cl, Br, or I) Prepared by Ball-Milling and Used as Anode Materials for Lithium-Ion Batteries. *Adv. Mater.,* **26**, 7317 (2014).

[25]. Zhan, L., Yang, S., Wang, Y., Wang, Y., Ling, L., Feng, X., Fabrication of Fully Fluorinated Graphene Nanosheets Towards High-Performance Lithium Storage. *Adv. Mater. Interfaces*, **1**, 1300149 (2014).

[26]. Jeon, I.-Y., Ju, M. J., Xu, J., Choi, H.-J., Seo, J.-M., Kim, M.-J., Choi, I. T., Kim, H. M., Kim, J. C., Lee, J.-J., Liu, H. K., Kim, H. K., Dou, S., Dai L., Baek, J.-B., Edge-Fluorinated Graphene Nanoplatelets as High Performance Electrodes for Dye-Sensitized Solar Cells and Lithium Ion Batteries. *Adv. Funct. Mater.,* **25,** 1170 (2015).

[27]. Ito, S., Wehmeier, M., Brand, J. D., Kübel, C., Epsch, R., Rabe J. P., Müllen, K., Synthesis and Self-Assembly of Functionalized Hexa-peri-hexabenzocoronenes. *Chem. Eur. J.,* **6**, 4327 (2000).

[28]. Tan, Y.-Z., Osella, S., Liu, Y., Yang, B., Beljonne, D., Feng X., Müllen, K. Sulfur-Annulated Hexa-peri-hexabenzocoronene Decorated with Phenylthio Groups at the Periphery. *Angew. Chem*., Int. Ed., **54**, 2927 (2015).

[29]. Swain, A. K., & Bahadur, D. Facile synthesis of twisted graphene solution from graphite-KCl. *RSC Advances*, **3**(42), 19243-19246 (2013).

[30]. Mkhalid, I. A. I., Barnard, J. H., Marder, T. B., Murphy, J. M., Hartwig, J. F., C− H activation for the construction of C− B bonds. *Chem. Rev.,* **110**, 890 (2009).

[31]. Mochida, K., Kawasumi, K., Segawa Y., Itami, K., Direct arylation of polycyclic aromatic hydrocarbons through palladium catalysis. *J. Am. Chem. Soc*., **133**, 10716 (2011).

[32]. Ozaki, K., Kawasumi, K., Shibata, M., Ito H., Itami, K. One-shot K-region-selective annulative π-extension for nanographene synthesis and functionalization. *Nat. Commun.,* **6**, 6251 (2015).

[33]. Kawasumi, K., Zhang, Q., Segawa, Y., Scott L. T., Itami, K. A grossly warped nanographene and the consequences of multiple odd-membered-ring defects. *Nat. Chem.,* **5**, 739 (2013).

[34]. Singh, P., Campidelli, S., Giordani, S., Bonifazi, D., Bianco, A., Prato, M. Organic functionalisation and characterisation of single-walled carbon nanotubes, *Chem. Soc. Rev.*, **38**, 2214–2230 (2009).

[35]. Chua, C. K., Pumera, M. Carbocatalysis: The State of "Metal-Free" Catalysis. *Chem. Eur. J.* **21**: 12550 – 12562 (2015).

[36]. Brodie, B.C. On the atomic weight of graphite. *Philos. Trans. R. Soc. Lond.* **14**: 249–259 (1859).

[37]. Lopez, M. I., Croce, A. E., Sicre, J. E. Explosive decomposition of gaseous chlorine dioxide. *J. Chem. Soc. Faraday Trans.* **90** (22): 3391–3396 (1994).

[38]. McAllister, M. J., Li, J.-L., Adamson, D. H., Schniepp, H. C., Abdala, A. A., Liu, J., Herrera-Alonso, M., Milius, D. L., Car, R., Prud'homme, R. K., Aksay, I. A. Single sheet functionalized graphene by oxidation and thermal expansion of graphite. *Chem. Mater.* **19** (18): 4396–4404 (2007).

[39]. Staudenmaier, L. Verfahren zur Darstellung der Graphitsäure. *Ber. Dtsch. Chem. Ges.* **31**: 1481-1487 (1898).

[40]. Hummers, W. S., Offeman, R. E. Preparation of Graphitic Oxide. *J. Am. Chem. Soc.* **80**: 1339-1339 (1958).

[41]. Ang, P. K., Wang, S., Bao, Q., Thong, J. T. L., Loh, K. P. High-throughput synthesis of graphene by intercalation–exfoliation of graphite oxide and study of ionic screening in graphene transistor. *ACS Nano* **3** (11): 3587–3594 (2009).

[42]. Chen, J., Yao, B., Li, C., Shi, G. An improved Hummers method for eco-friendly synthesis of graphene oxide. *Carbon* **64**: 225–229 (2013).

[43]. Chen, J., Li Y., Huang, L., Li, C., Shi, G. High-yield preparation of graphene oxide from small graphite flakes via an improved Hummers method with a simple purification process. *Carbon* **81**: 826–834 (2015).

[44]. Guerrero-Contreras, J., Caballero-Briones, F. Graphene oxide powders with different oxidation degree, prepared by synthesis variations of the Hummers method. *Mater. Chem. Phys.* **153**: 209-220 (2015).

[45]. Kovtyukhova, N. I., Ollivier, P. J., Martin, B. R., Mallouk, T. E., Chizhik, S. A., Buzaneva, E. V., Gorchinskiy, A. D. Layer-by-layer assembly of ultrathin composite films from micron-sized graphite oxide sheets and polycations. *Chem. Mater.* **11** (3): 771–778 (1999).

[46]. Grennberg, H., Jansson, U. Synthesis of Graphene and Derivatives. Science and Technology of Atomic, Molecular, *Condensed Matter & Biological Systems* **2**: 105–127 (2012).

[47]. Zhu, Y., Murali, S., Cai, W., Li, X., Suk, J. W., Potts, J. R., Ruoff, R. S. Graphene And Graphene Oxide: Synthesis, Properties, And Applications. *Adv. Mater.* **22**: 3906–3924 (2010).

[48]. Jeon, I. Y., Bae, S. Y., Seo, J. M., & Baek, J. B. Scalable Production of Edge-Functionalized Graphene Nanoplatelets via Mechanochemical Ball-Milling. *Advanced Functional Materials*, **25**(45), 6961-6975 (2015).

[49]. Mauro, M., Cipolletti, V., Galimberti, M., Longo, P., & Guerra, G. Chemically reduced graphite oxide with improved shape anisotropy. *The Journal of Physical Chemistry C*, **116**(46), 24809-24813 (2012).

[50]. Yan, L., Lin, M., Zeng, C., Chen, Z., Zhang, S., Zhao, X., & Guo, M. Electroactive and biocompatible hydroxyl-functionalized graphene by ball milling. *Journal of Materials Chemistry*, **22**(17), 8367-8371 (2012).

[51]. Barbera, V., Porta, A., Brambilla, L., Guerra, S., Serafini, A., Valerio, A. M., & Galimberti, M. Polyhydroxylated few layer graphene for the preparation of flexible conductive carbon paper. *RSC Advances*, **6**(90), 87767-87777 (2016).

[52]. Vibhute, Y. B., Lonkar, S. M., Sayyed, M. A., & Baseer, M. A. Synthesis of substituted 2-hydroxyaryl aldehydes by the microwave-induced Reimer-Tiemann reaction. *Mendeleev Communications*, **17**(1), 51 (2007).

[53]. Crisan, R., & Modra, D. The synthesis of salicylaldehyde varying different parameters. *Annals of West University of Timisoara. Series of Chemistry*, **22**(2), 57 (2013).

[54]. Hine, J., & Van Der Veen, J. M. The Mechanism of the Reimer-Tiemann Reaction[1]. *Journal of the American Chemical Society*, **81**(24), 6446-6449 (1959).

[55]. Corsaro, A., Chiacchio, U., Adamo, R., Pistarà, V., Rescifina, A., Romeo, R., ... & Attolino, E. Steric course of some cyclopropanation reactions of L-threo-hex-4-enopyranosides. *Tetrahedron*, **60**(17), 3787-3795 (2004).

[56]. Chua, C. K., Ambrosi, A., & Pumera, M. (2012). Introducing dichlorocarbene in graphene. *Chemical Communications*, *48*(43), 5376-5378.

[57]. Simmons, H. E., & Smith, R. D. (1958). A new synthesis of cyclopropanes from olefins. *Journal of the American Chemical Society*, *80*(19), 5323-5324.

[58]. Simmons, H. E., Cairns, T. L., Vladuchick, S. A., & Hoiness, C. M. (1973). Cyclopropanes from Unsaturated Compounds, Methylene Iodide, and Zinc-Copper Couple. *Organic Reactions*.

[59]. Pistarà, V., Rescifina, A., Punzo, F., Greco, G., Barbera, V., & Corsaro, A. (2011). Design, Synthesis, Molecular Docking and Crystal Structure Prediction of New Azasugar Analogues of α-Glucosidase Inhibitors. *European Journal of Organic Chemistry*, *2011*(36), 7278-7287.

766 [60]. Sauers, R. R., Schlosberg, S. B., & Pfeffer, P. E. (1968). Synthesis and chemistry of some
767 tricyclo [4.2. 1.02, 5] nonane derivatives. *The Journal of Organic Chemistry*, *33*(6), 2175-
768 2181.
769 [61]. Pearl, I. A. Reactions Of Vanillin And Its Derived Compounds. Iii. 1 The Cannizzaro
770 Reaction Of Vanillin[2]. *The Journal of organic chemistry*, **12**(1), 79-84 (1947).
771 [62]. Pearl, I. A. Silver Catalyzed Reactions Of Phenolic Aldehydes[1]. *The Journal of organic*
772 *chemistry*, **12**(1), 85-89 (1947).
773 [63]. Rusling, J. F., Segretario, J. P., & Zuman, P. Polarographic reduction of aldehydes and
774 ketones: Part XXIII. Electroreduction of 1-methylpyridiniumcarboxaldehydes. *Journal of*
775 *Electroanalytical Chemistry and Interfacial Electrochemistry*, **143**(1-2), 291-321 (1983).
776 [64]. Soria-Sánchez, M., Maroto-Valiente, A., Álvarez-Rodríguez, J., Mu˜noz-Andrés, V.,
777 Rodríguez-Ramos, I., Guerrero-Ruíza, A., Carbon nanostrutured materials as direct catalysts
778 for phenol oxidation in aqueous phase. *Applied Catalysis B: Environmental,* **104,** 101–109
779 (2011).
780 [65]. Galimberti, M., Barbera, V., Guerra, S., Conzatti, L., Castiglioni, C., Brambilla, L., &
781 Serafini, A. Biobased Janus molecule for the facile preparation of water solutions of few layer
782 graphene sheets. *RSC Advances*, ***5***(99), 81142-81152 (2015).
783 [66]. Barbera V., Guerra S., Brambilla L., Maggio M., Serafini A., Conzatti L., ... & Galimberti
784 M., Carbon papers and aerogels based on graphene layers and chitosan: direct preparation
785 from high surface area graphite. *Biomacromolecules*, **2017**, 18(12), 3978–3991.
786 [67]. Socrates, G. Infrared Characteristic Group Frequencies, 2nd ed.; Wiley: New York (1980).
787 [68]. Boczar, M., Wójcik, M. J., Szczeponek, K., Jamróz, D., Ikeda, S., Theoretical Modeling of
788 Infrared Spectra of Salicylaldehyde and Its Deuterated Derivatives, *International Journal of*
789 *Quantum Chemistry*, **90**, 689–698 (2002)
790 [69]. Yang, D., Velamakanni, A., Bozoklu, G., Park, S., Stoller, M., Piner, R. D., ... & Ruoff, R.
791 S. Chemical analysis of graphene oxide films after heat and chemical treatments by X-ray
792 photoelectron and Micro-Raman spectroscopy. *Carbon*, **47**(1), 145-152 (2009).
793 [70]. Gustafsson, J. B., Moons, E., Widstrand, S. M., Gurnett, M., & Johansson, L. S. O. Thin
794 PTCDA films on Si (001): 2. Electronic structure. *Surface science*, **572**(1), 32-42 (2004).
795 [71]. Ferrari, A. C., Robertson, J., Raman spectroscopy of amorphous, nanostructured, diamond-
796 like carbon, and nanodiamond. *Phil. Trans. R. Soc. Lond. A* **362**, 2477–2512 (2004).
797 [72]. Dresselhaus, M. S. Intercalation compounds of graphite, *Advances in Physics*, **51**(1) 1-186
798 (2002).

[73]. Alsmeyer, D. C. et al. In situ Raman monitoring of electrochemical graphite intercalation and lattice damage in mild aqueous acids. *Anal. Chem.*, **64**, 1528-1533 (1992).

[74]. Dimiviev, A.M. et al. Reversible formation of ammonium persulfate/sulfuric acid graphite intercalation compounds and their peculiar Raman spectra. *ACS Nano*, **6**(9), 7842–7849 (2012).

[75]. Andrea C. Ferrari, Raman spectroscopy of graphene and graphite: Disorder, electron–phonon coupling, doping and nonadiabatic effects Solid State Communications 143 (2007)

[76]. Ferrari, A. C. Raman spectroscopy of graphene and graphite: disorder, electron–phonon coupling, doping and nonadiabatic effects. Solid state communications, 143(1-2), 47-57, (2007).

[77]. Zhao, W., Tan, P., Zhang, J., & Liu, J. Charge transfer and optical phonon mixing in few-layer graphene chemically doped with sulfuric acid. Physical Review B, 82(24), 245423 (2010).

[78]. Swain, A. K., & Bahadur, D. Facile synthesis of twisted graphene solution from graphite-KCl. *RSC Advances*, ***3***(42), 19243-19246 (2013).

[79]. Corsaro, A., Chiacchio, M. A., Pistarà, V., Rescifina, A., & Vittorino, E. (2008). Cyclopropanation of 5-methylene galactopyranosides by dihalo-, ethoxycarbonyl-, and unsubstituted carbenes. *Tetrahedron*, **64**(37), 8652-8658.

[80]. Tozzini, V., & Pellegrini, V. Prospects for hydrogen storage in graphene. *Physical Chemistry Chemical Physics*, ***15***(1), 80-89 (2013).

[81]. Q. Wang; B. Zhang; X. Lin; W. Weng. Hybridization biosensor based on the covalent immobilization of probe DNA on chitosan–mutiwalled carbon nanotubes nanocomposite by using glutaraldehyde as an arm linker *Sensors and Actuators B: Chemical* **2011**, 156, 599–605

[82]. Hung W. S.; Chang S. M.; Lecaros R. L. G.; Ji Y. L.; An Q. F.; Hu C. C.; Lee K. R.; Lai J. Y. Fabrication of hydrothermally reduced graphene oxide/chitosan composite membranes with a lamellar structure on methanol dehydration Carbon **2017**, 117, 112-119.

[83]. Tabasi A.; Noorbakhsh A.; Sharifi E. Reduced graphene oxide-chitosan-aptamer interface as new platform for ultrasensitive detection of human epidermal growth factor receptor 2. *Biosensors and Bioelectronics* **2017**, 95, 117-123

[84]. Peng Yua P.; Bao R. Y.; Shi X. J.; Yang W.; Yanga M.B. Self-assembled high-strength hydroxyapatite / graphene oxide / chitosan composite hydrogel for bone tissue engineering *Carbohydrate Polymers* **2017**, 155, 507–515

832 [85]. Brugnerotto J., Lizardi J., Goycoolea F.M., Argüelles-Monal W., Desbrières J., M.
833 Rinaudo, An infrared investigation in relation with chitin and chitosan characterization
834 *Polymer* 2001, 42, 3569-3580.
835